

Automatic Optic Disk Segmentation in Presence of Disk Blurring

Samra Irshad^{1(✉)}, Xiaoxia Yin², Lucy Qing Li^{3,4}, and Umer Salman⁵

¹ The Superior College, University Campus, Lahore, Pakistan
sam.ershad@yahoo.com

² Centre for Applied Informatics, College of Engineering and Science,
Victoria University, Melbourne, Australia
xiaoxia.yin@vu.edu.au

³ College of Engineering and Science, Victoria University, Melbourne, Australia

⁴ EEC Bio-tech Co. Ltd., Guangzhou, China

⁵ Hameed Latif Hospital, Lahore, Pakistan

Abstract. Fundus image analysis has emerged as a very useful tool to analyze the structure of retina for detection of different eye-related abnormalities. The detection of these abnormalities requires the segmentation of basic retinal structures including blood vessels and optic disk. The optic disk segmentation becomes a challenging task when the optic disk boundary is degraded due to some deviations including optic disk edema and papilledema. This paper focuses on the segmentation of optic disk in presence of disk blurring. The method proposed makes use of gradient extracted from line profiles that pass through optic disk margin. Initially the optic disk is enhanced using morphological operations and location of optic disk region is detected automatically using vessel density property. Finally, line profiles are extracted at different angles and their gradient is evaluated for the estimation of optic disk boundary. The proposed method has been applied on 28 images taken from Armed Forces Institute of Ophthalmology.

1 Introduction

Health surveys show approximately 40% of world population above the age of 25 has hypertension [1]. Systematic hypertension manifests ocular effects in retina, choroid and optic nerve [2]. The changes and abnormalities that are caused in retina due to hypertension can be detected and diagnosed by non-mydriatic retinal photography [2].

Computerized Automatic Diagnostic (CAD) systems are being developed for the past decade to detect different ocular diseases. These CAD systems not only alleviate the burden on ophthalmologists but also provide them with a second independent opinion. Majority of the systems which have been proposed for the detection of changes caused by hypertension like the quantification of blood vessels include the segmentation of the basic retinal structures like Optic Disk (OD) and retinal blood vessels as a preliminary step [3–6]. OD usually appears as a bright yellow circular structure from where the retinal vessels emerge, however this feature may vary across images significantly as shown in Fig. 1. Also, OD boundary is sometimes not clear enough due to

other abnormalities like Optic Disk Edema and Papilledema, as shown in Fig. 2. These variations and other complications make the segmentation of OD difficult.

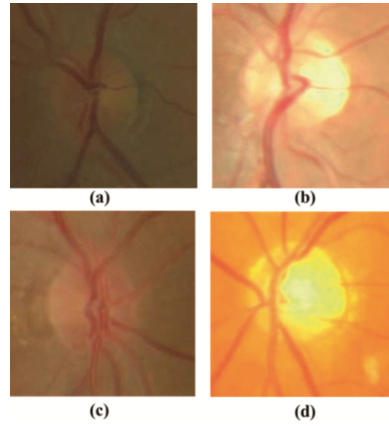


Fig. 1. Variations in appearance of OD: (a) Brownish OD image, (b) Whitish OD, (c) Reddish OD, (d) Yellowish OD. (Color figure online)

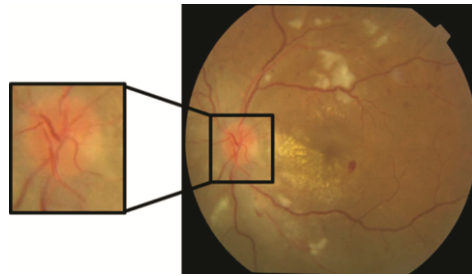


Fig. 2. Example of OD blurring

This paper presents a novel method for OD boundary segmentation in retinal fundus images with OD disk swelling. The proposed technique works correctly for images in which the OD boundary is blurred secondary to changes caused by malignant hypertension. The long-term high blood pressure can lead to raised intracranial pressure which is another reason for OD swelling [7–9]. Along with the obscured boundary, the color of OD also changes from bright to abnormally pale as shown in Fig. 2. This paper contains four sections. A review of previous methods is given in Sect. 2, Sect. 3 describes the proposed methodology, Sect. 4 shows experimental results followed by conclusion that is given in Sect. 5.

2 Related Work

The techniques which have been proposed so far segment the optic nerve head in absence of OD blurring. D. Marin et al. [10] presented a method for OD segmentation which includes the application of morphological operations followed by Hough transform. Circular Hough transform is also used in [11] for OD center approximation and grow cut algorithm for boundary segmentation. Another method presented in [12] used Principal Component Analysis (PCA) for detection of OD and active contour model is proposed for OD boundary segmentation. C. Wang et al. presented a work in which template matching is used to detect OD center followed by Level Set Method for boundary segmentation [13]. Region growing algorithm is used in [14] for segmentation of OD boundary. Recently a research is presented in [15], for detection of OD in presence of pathologies like exudates.

This paper contributes in correct detection and segmentation of OD in presence of retinal pathology i.e. OD blurring. OD blurring makes the identification and boundary segmentation of OD ambiguous because of its resultant effects.

3 Proposed Method

The proposed technique consists of four stages; Preprocessing, Vessel Segmentation, OD detection and Line profiles extraction followed by evaluation of maximum gradient along line profiles. In the first stage, preprocessing is applied on fundus image followed by segmentation of retinal vessels. In the second step, retinal vessels are segmented using Gabor Wavelet. In the third step, OD position is localized using Laplacian of Gaussian filter and highest vessel property of OD. Then, the center of detected OD region

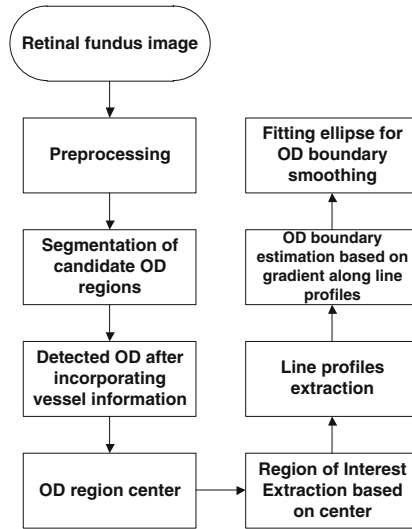


Fig. 3. Flow chart of proposed methodology

is found and based on that center; a region of interest is extracted containing the OD portion. Finally, line profiles are extracted at several orientations which pass through the OD region's center. The gradient along these profiles are recorded and the pixels with maximum gradient are marked. These pixels provide a basis for OD boundary detection and are used to fit an ellipse. The proposed methodology is tested on images gathered from AFIO, Pakistan. A comparison is also made with the ground truth OD masks. Figure 3 shows the flow diagram of proposed method. The steps adopted in the method are described in detail in this section.

3.1 Background Segmentation

In preprocessing, the fundus background is removed in order to suppress un-necessary pixels. The reason for this removal is that the dark background is not actually black. Background estimation is done using local mean and variance based method [16]. Then, thresholding and morphological operations are applied to create a binary mask. The original image along with background segmentation is shown in Fig. 4.

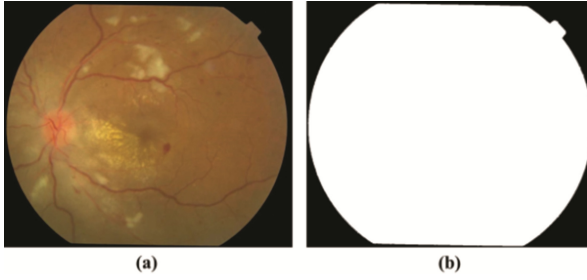


Fig. 4. Background segmentation: (a) Original fundus image, (b) Background mask

3.2 Vessel Segmentation

For segmentation of vessels, 2-Dimensional Gabor Wavelet is used [17]. The purpose of using Gabor filter is their localization property, they capture the response of small as well large width vessels with greater accuracy. After enhancement, retinal vessels are thresholded. Equation 1 shows expression for Gabor Wavelet, which is simply a multiplication of complex exponential and 2-D Gaussian sinusoidal [18].

$$G(x, y) = \frac{1}{2\pi\sigma\beta} e^{-\pi\left[\frac{(x-x_0)^2}{\sigma^2} + \frac{(y-y_0)^2}{\beta^2}\right]} e^{i[\delta_0 x + \theta_0 y]} \quad (1)$$

Gabor Wavelet response is evaluated for various orientations spanning from 0° up to 179° at steps of 10° and then their maximum response is taken [17]. A Gabor Wavelet enhanced retinal image is shown in Fig. 5 (a) along with its thresholded version in Fig. 5 (b).

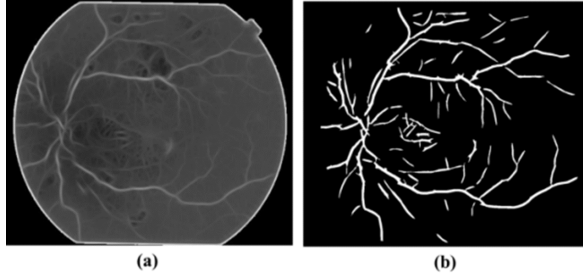


Fig. 5. Vessel segmentation: (a) Retinal vessel enhancement, (b) Segmented retinal vessel network

3.3 Localization of the Position of OD

In the proposed system, Laplacian of Gaussian (LoG) filter and highest vessel density property of OD is used to detect the location of OD [19]. Red channel of RGB image is selected and a circular-shaped inverted LoG filter is used to enhance the location of OD [19]. This template is particularly used because of circular structure of OD. Red channel of image and LoG filter is shown in Fig. 6 below. The Red channel has been selected because it provides the clear and discriminating visualization of OD.

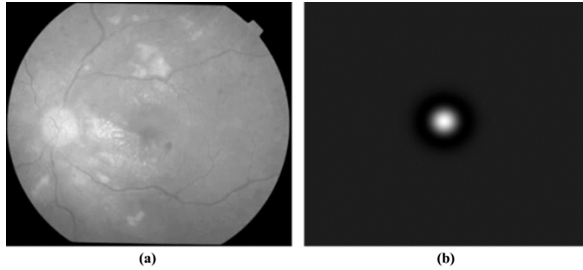


Fig. 6. Optic Disk detection: (a). Red channel of image (b). LoG filter. (Color figure online)

After the candidate circular regions have been enhanced using the LoG filter, they are binarized. The threshold that is used for this binarization is given in Eq. 2 [19]. $mLoG$ is the maximum value in LoG filtered image in Eq. 2.

$$T = 0.6 * mLoG \quad (2)$$

This threshold selects pixels having top 60% response from the LoG filtered image [19]. Preliminary experiment guided the selection of this threshold since it is optimal for all the images. Images in the dataset contain pathologies like exudates and cotton wool spots that have similarity in structural and color properties with OD, so the LoG filtered and subsequent thresholded image may contain more than one OD region. To overcome this issue, vessel density property is incorporated to separate out the OD region from the other segmented portions. A bounding box is drawn around these

regions, and vessel density inside them is evaluated. The region with maximum vessel variation is selected. Figure 7 shows the complement of segmented vessel image with bounding box created around OD candidate regions.

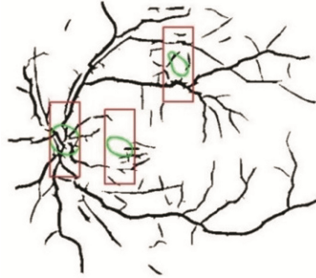


Fig. 7. Bounding boxes marked on candidate OD regions

Figure 8 shows the extracted candidate regions after thresholding with LoG filter and the OD region after incorporating vessel density characteristic. After determination of OD region, its center is evaluated and a sub-image containing OD is extracted. This sub-image is of dimensions 500×620 and is extracted by taking into account the center of OD region as shown in Fig. 9. This sub-image is used as input data for OD boundary estimation.

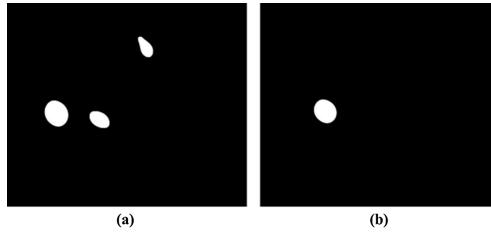


Fig. 8. Localization of OD region: (a). Segmented candidate OD regions (b). OD region after using vessel information

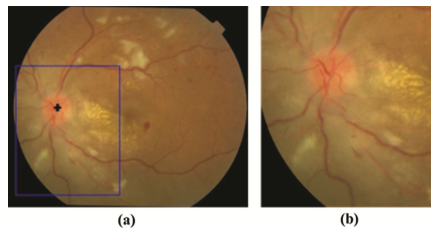


Fig. 9. Determination of ROI: (a). ROI marked in blue box and center of detected OD's region marked in black, (b). ROI region. (Color figure online)

3.4 Boundary Detection of OD by Variation Along Line Profile

In our dataset, the OD region has the most discriminating appearance in the red color plane, as mentioned before. However, in some sub-images, the fundus regions other than OD appears brighter due to intra-image variations and makes the appearance of OD as non-discriminating in red channel. Therefore, a mean threshold is chosen which determines the selection of color channel. If the mean threshold value of RGB sub-image is equal or greater than 130, blue color plane is selected as input image otherwise red component is chosen. Afterwards, the line segments of specific length are used to determine the pixels with highest gradient, which will lead to the evaluation of OD boundary. Radial line segments l_i with the length of 120 are taken at several orientations and regular intervals i.e. from $\theta = 0^\circ$ to 180° with the step of 10° that pass through the center of OD region. The length of the line segments is made such that it is long enough to capture the variation on OD boundary. The profiles across the line segments are evaluated and then their 1-D gradient is calculated. The absolute of this gradient is taken since the lowest negative value indicates the variation along the region of high intensity to low intensity and highest positive value of gradient indicates the variation of low to high intensity [20]. The location of these gradient values is obtained and marked.

The intensity inside the OD is not uniform due to the presence of vessel structures, therefore in some cases the gradient shows prominent variations not only at OD margins but also inside the OD region. To avoid this situation, the Euclidean distance is measured from the detected points to the center of region and the mean of all calculated distances is taken. If the distance from the coordinates of maximum variation point and center is less than mean value; the detected gradient point is discarded. After discarding the points that have less distance than the selected mean threshold, a boundary is traced that follows the retained gradient points. Moreover, as the blood vessel emerge from OD center and crosses the boundary, this vessel crossing characteristic will prevent the gradient-based method in tracing the smooth boundary. For this purpose, ellipse fitting is applied to the detected points in order to smooth the traced boundary [21]. Figure 10 (a) shows the selected component of RGB image with radial segments and detected points on OD boundary, (b) represents the ellipse fitted boundary and (c) shows the obtained binary mask. Figure 11 shows results of proposed methodology on two images. Note the OD boundary in colored

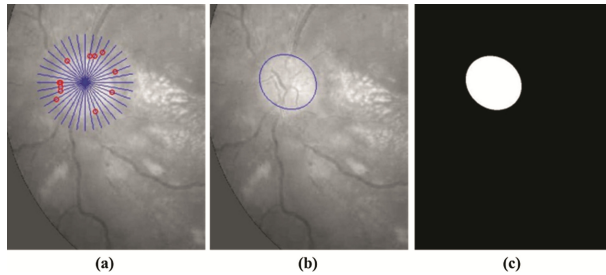


Fig. 10. OD detection: (a). Detected points of blurred OD margin, (b). Ellipse fitting to points, (c) resultant mask. (Color figure online)

image in the first row is blurred at temporal side, while in the second image; the vessels are twisted due to tortuosity which resulted in OD boundary distortion.

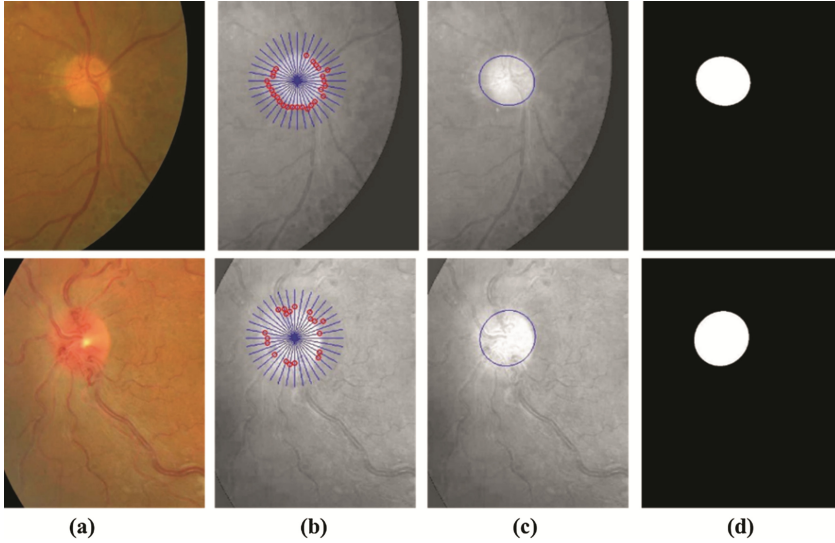


Fig. 11. Boundary segmentation of OD: (a). Colored sub-images (b). Selected channel for boundary segmentation with line segments and detected points superimposed, (c). Ellipse fitting to detected points, (d). Generated binary mask. (Color figure online)

4 Results

A dataset of 28 images is used for testing of proposed methodology. These images are of size 1504×1000 , taken from Ophthalmology department of AFIO, Pakistan. The OD in these images has been annotated as ‘blurring present’ or ‘not’ by an experienced ophthalmologist. The OD boundary in the images has been annotated by our ophthalmologist and those annotations are then used as ground truth. Among the 28 images, 9 of them contain OD swelling.

In this paper, three performance measures are used for the performance evaluation of proposed method. Jaccard and Dice coefficients shown in Eqs. 3 and 4 are used to evaluate the OD boundary segmentation results whereas the third measure is the Euclidean distance between the center of OD obtained from the proposed method and ground truth masks is used to evaluate the localization of OD center [22]. Jaccard coefficient (JC_{seg}) is defined as the intersection divided by union of the OD segmentation resulted from the proposed system (S_{test}) and the ground truth segmentation (S_{gr}). While the Dice Coefficient (DC_{seg}) is about the size of the intersection of the OD boundary segmentation resulted from the proposed system (S_{test}) and the ground truth segmentation (S_{gr}) divided by their average size.

$$JC_{seg} = \frac{S_{test} \cap S_{gt}}{S_{test} \cup S_{gt}} \quad (3)$$

$$DC_{seg} = \frac{2 \cdot S_{test} \cap S_{gt}}{S_{test} + S_{gt}} \quad (4)$$

Table 1 shows the results of performance evaluation for OD boundary segmentation. The average values achieved for JC_{seg} , DC_{seg} and distance between OD centers are 0.8331, 0.9078 and 6.44, respectively.

Table 1. Performance of evaluation parameters for 28 images

Image no.	(JC_{seg})	(DC_{seg})	$(Dist)$
1	0.8539	0.9212	9.0554
2	0.8282	0.906	9.2195
3	0.854	0.9213	7
4	0.7836	0.8787	8.2462
5	0.695	0.82	2.2361
6	0.8365	0.9109	4.1231
7	0.9489	0.9738	2.8284
8	0.7172	0.8353	12.083
9	0.7377	0.8491	7.2801
10	0.9036	0.9493	2.8284
11	0.7896	0.8824	7.2111
12	0.8364	0.9109	7.2801
13	0.8565	0.9227	4
14	0.8041	0.8914	9.2195
15	0.8206	0.9015	10.6301
16	0.9046	0.9499	4.4721
17	0.829	0.9065	4
18	0.8478	0.9176	7.6158
19	0.7725	0.8716	4.4721
20	0.8788	0.9355	7.2111
21	0.8795	0.9359	5.6569
22	0.8166	0.899	10
23	0.8796	0.9359	5
24	0.7775	0.8748	8.0623
25	0.8139	0.8974	11.6619
26	0.9026	0.9488	1
27	0.8861	0.9396	3.1623
28	0.8743	0.9329	5

5 Conclusion

This paper presents an improved method for the segmentation of OD in colored retinal images with pathological degradations. A gradient based method is proposed for the OD boundary segmentation, which consists of maximum gradient pixels extraction followed by ellipse fitting. This technique provides accuracy for images with OD margin blurred. The algorithms which have been proposed so far [10–15] provide OD segmentation in normal images.

References

1. World Health Organization: A Global Brief on Hypertension. World Health Organization, Geneva (2013)
2. Hyman, B.N., Moser, M.: Hypertension update. *Surv. Ophthalmol.* **41**, 79–89 (1996)
3. Agurto, C., Joshi, V., Nemeth, S., Soliz, P., Barriga, S.: Detection of hypertensive retinopathy using vessel measurements and textural features. In: 36th Annual International Conference of the IEEE EMBS. IEEE Press, Chicago (2014)
4. Yin, X., Ng, B.W.-H., He, J., Zhang, Y., Abbott, D.: Accurate image analysis of the retina using Hessian matrix and binarisation of thresholded entropy with application of texture mapping. *PLoS ONE* **9**(4), e95943 (2014)
5. Irshad, S., Usman Akram, M., Ayub, S., Ayaz, A.: Retinal blood vessels differentiation for calculation of arterio-venous ratio. In: Kamel, M., Campilho, A. (eds.) *ICIAR 2015. LNCS*, vol. 9164, pp. 411–418. Springer, Heidelberg (2015). doi:[10.1007/978-3-319-20801-5_45](https://doi.org/10.1007/978-3-319-20801-5_45)
6. Irshad, S., Usman Akram, M.: Classification of retinal vessels into arteries and veins for detection of hypertensive retinopathy. In: *IEEE 7th Cairo International Biomedical Engineering Conference (CIBEC)*. IEEE Press, Egypt (2014)
7. Auer, R.N., Sutherland, G.R.: Primary intracerebral hemorrhage: pathophysiology. *Can. J. Neurol. Sci.* **32**, S3–S12 (2005)
8. Sahni, R., Weinberger, J.: Management of intracerebral hemorrhage. *J. Vasc. Health Risk Manag.* **3**, 701 (2008)
9. Agarwal, S., Agarwal, A., Apple, D.J., Buratto, L., Alio, J.L.: *Textbook of Ophthalmology*, vol. 1, Jaypee Brothers Medical Publishers (2002)
10. Marin, D., Arias, M.E.G., Suero, A., Bravo, J.M.: Obtaining optic disc center and pixel region by automatic thresholding methods on morphologically processed fundus images. *Comput. Meth. Programs Biomed.* **118**, 173–185 (2015)
11. Abdullah, M., Fraz, M.M.: Application of grow cut algorithm for localization and extraction of optic disc in retinal images. In: *12th International Conference on High-Capacity Optical Networks and Emerging Technologies (HONET)*. IEEE Press (2015)
12. Mittapalli, P.S., Kande, G.B.: Segmentation of optic disk and optic cup from digital fundus images for the assessment of glaucoma. *Biomed. Sig. Process. Control* **24**, 34–46 (2016)
13. Wang, C., Kaba, D., Li, Y.: Level set segmentation of optic discs from retinal images. *J. Med. Bioeng.* **4**, 213–220 (2015)
14. Omid, S., Ghassabi, Z., Shanbehzadeh, J., Ostadzadeh, S.S.: Optic disc detection in high-resolution retinal fundus images by region growing. In: *8th International Conference on BioMedical Engineering and Informatics (BMEI)*. IEEE Press (2015)
15. Xiong, L., Li, H.: An approach to locate optic disc in retinal images with pathological changes. *Comput. Med. Imaging Graph.* **47**, 40–50 (2016)

16. Jamal, I., Akram, M.U., Tariq, A.: Retinal image preprocessing: background and noise segmentation. *TELKOMNIKA* **10**(3), 537–544 (2012)
17. Akram, M.U., Jamal, I., Tariq, A.: Blood vessel enhancement and segmentation for screening of diabetic retinopathy. *TELKOMNIKA Indonesian J. Electr. Eng.* **10**, 327–334 (2012)
18. Lee, T.S.: Image representation using 2D Gabor wavelets. *IEEE Trans. Pattern Anal. Mach. Intell.* **18**(10), 959–971 (1996)
19. Usman, A., Khitran, S.A., Usman Akram, M., Nadeem, Y.: A robust algorithm for optic disc segmentation from colored fundus images. In: Campilho, A., Kamel, M. (eds.) *ICIAR 2014*. LNCS, vol. 8815, pp. 303–310. Springer, Heidelberg (2014). doi:[10.1007/978-3-319-11755-3_34](https://doi.org/10.1007/978-3-319-11755-3_34)
20. Gonzales, R.C., Woods, R.E.: *Digital Image Processing*, 3rd edn. Prentice-Hall, Upper Saddle River (2008)
21. Stojmenovic, M., Nayak, A.: Direct ellipse fitting and measuring based on shape boundaries. In: Mery, D., Rueda, L. (eds.) *PSIVT 2007*. LNCS, vol. 4872, pp. 221–235. Springer, Heidelberg (2007). doi:[10.1007/978-3-540-77129-6_22](https://doi.org/10.1007/978-3-540-77129-6_22)
22. Nikravesh, M., Zadeh, L.A.: *Soft Computing for Information Processing and Analysis*. Springer-Verlag, Heidelberg (2005)

Advances in Visual Computing

12th International Symposium, ISVC 2016, Las Vegas,

NV, USA, December 12-14, 2016, Proceedings, Part I

Bebis, G.; Boyle, R.; Parvin, B.; Koracin, D.; Porikli, F.;

Skaff, S.; Entezari, A.; Min, J.; Iwai, D.; Sadagic, A.;

Scheidegger, C.; Isenberg, T. (Eds.)

2016, XXXVI, 873 p. 392 illus., Softcover

ISBN: 978-3-319-50834-4